ACS APPLIED MATERIALS & INTERFACES

Research Article

www.acsami.org

Biomimetic Mineralization of Recombinamer-Based Hydrogels toward Controlled Morphologies and High Mineral Density

Yuping Li,*,† Xi Chen,† Alex Fok,† Jose Carlos Rodriguez-Cabello,‡ and Conrado Aparicio*,†

†Minnesota Dental Research Center for Biomaterials and Biomechanics, University of Minnesota, Minneapolis, Minnesota 55455, United States

‡GIR Bioforge, University of Valladolid, Valladolid 47002, Spain

Supporting Information

ABSTRACT: The use of insoluble organic matrices as a structural template for the bottom-up fabrication of organic−inorganic nanocomposites is a powerful way to build a variety of advanced materials with defined and controlled morphologies and superior mechanical properties. Calcium phosphate mineralization in polymeric hydrogels is receiving significant attention in terms of obtaining biomimetic hierarchical structures with unique mechanical properties and understanding the mechanisms of the biomineralization process. However, integration of organic matrices with hydroxyapatite nanocrystals, different in morphology and composition, has not been well-achieved yet at nanoscale. In this study, we synthesized thermoresponsive hydrogels, composed of elastin-like recombinamers (ELRs), to template mineralization of hydroxyapatite nanocrystals using a biomimetic polymer-induced liquid-precursor (PILP) mineralization process. Different from conventional mineralization where minerals were deposited on the surface of organic matrices, they were infiltrated into the frameworks of ELR matrices, preserving their microporous structure. After 14 days of mineralization, an average of 78 μm mineralization depth was achieved. Mineral density up to 1.9 g/cm^3 was found after 28 days of mineralization, which is comparable to natural bone and dentin. In the dry state, the elastic modulus and hardness of the mineralized hydrogels were 20.3 ± 1.7 and 0.93 ± 0.07 GPa, respectively. After hydration, they were reduced to 4.50 ± 0.55 and 0.10 ± 0.03 GPa, respectively. These values were lower but still on the same order of magnitude as those of natural hard tissues. The results indicated that inorganic−organic hybrid biomaterials with controlled morphologies can be achieved using organic templates of ELRs. Notably, the chemical and physical properties of ELRs can be tuned, which might help elucidate the mechanisms by which living organisms regulate the mineralization process.

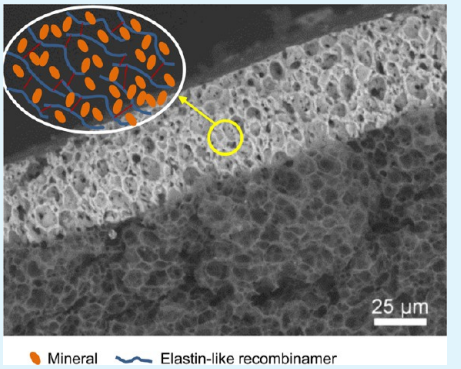

KEYWORDS: *mineralization, elastin-like recombinamers, hydrogel, bone, dentine*

1. INTRODUCTION

Hard tissues are organic−inorganic nanocomposites that exhibit remarkable mechanical properties with hierarchical structures.[1,2] In bone, a small amount of acidic noncollagenous proteins (NCPs) and the self-assembled collagen fibrils play critical roles in mineralization.[3,4] Many of the NCPs are highly negatively charged, abundant with carboxylate groups from aspartic and glutamic acid residues or phosphate groups from phosphoserine. They stabilize the initial amorphous calcium phosphate (ACP) precursor phase, facilitate the precursor ion infiltration into collagen fibrils, and mediate mineral phase transformation.[5−8] Several studies have indicated that collagen fibrils provide a structural template where the interstitial spaces in the fibrils serve as confined compartments for mineral deposition,[4,9−12] i.e., the ACP nanoclusters infiltrate into the collagen fibrils and crystallize into oriented hydroxyapatite (HA) nanocrystals with their [001] direction parallel to the long axes of the collagen fibrils.[3]

Although extensive research has been performed on collagen-based mineralization, it should be noted that collagen matrices can only be obtained from natural sources.[4,48−50] There are concerns with disease transmission and immunogenic response. The organization of collagen molecules is also very sensitive to the processing conditions.[51] Only collagen fibrils with banding patterns can be mineralized in a way that the minerals infiltrate within them.[52] Other natural macromolecules and synthetic polymers, such as chitosan, polycaprolactone, polylactide, and Pluronic, have been used as organic matrices for apatite mineralization.[40,53−55] However, mineralization of these 3D bulk scaffolds using traditional crystallization processes, such as incubation in simulated body fluid (SBF), often resulted in the heterogeneous nucleation of HA on the surface of substrates or loosely trapped within porous scaffolds,[13,16,17] compromising their structural integrity as distinct organic and inorganic phases are formed. Such a scenario is also different from that of mature bone, which is composed of two continuous organic and

Received: August 18, 2015
Accepted: October 30, 2015

DOI: 10.1021/acsami.5b07628
ACS Appl. Mater. Interfaces XXXX, XXX, XXX−XXX

inorganic phases that determine its superior mechanical properties.[18]

In biologically controlled mineralization, the living organism controls the mineralization process directly or indirectly to produce biominerals with selected size, morphology, and structure.[19,20] The elaborate biomineral morphologies may result from the complexity of the template; i.e., the transient amorphous clusters accrete into the insoluble organic template and "mold" into the 3D structure of the matrix.[21−23] It is believed that the development of organic−inorganic nanocomposites on a large scale with complex 3D morphologies can only be achieved via a templating process, where the shape of the template defines the form of the final material.[20] The fluidic character of the amorphous precursor phases has many advantages for generating complex morphologies.[23] It has been shown that amorphous calcium carbonates can adapt to the shape of a polymeric matrix that mimicked the structure of the organic matrix in living organisms.[22,24,25] Calcite crystals can be molded into complex 2D and 3D structures thru the polymer-induced liquid-precursor (PILP) process, which has proven to be the underpinning mechanism of shape control in biomineralization.[22] Combination of the process with various substrates, templates, or compartments may build a variety of biomimetic structures useful for hard tissue engineering.[22]

Elastin is an extracellular matrix protein that is known for providing elasticity to tissues and organs, such as blood vessels, elastic ligaments, lung, and skin.[26,27] Elastin-like recombinamers (ELRs) are biosynthetic recombinant polypeptides based on a repeating pentapeptide sequence derived from tropoelastin, (VPG-Xaa-G), where Xaa is a guest amino acid (excluding proline).[28] One of the unique properties of these recombinamers is their inverse transition temperature (T_t) that allows them to transit between a soluble form at temperatures below T_t and an insoluble aggregation at temperatures above T_t.[29] Although mineralization of ELRs has been investigated by directly mixing them with minerals or incubating them in conventional mineralization solutions,[30] the role of ELRs in calcium phosphate mineralization has not been well explored.

Here, we demonstrated that ELR-based hydrogels can be mineralized through a biomimetic mineralization process by which the minerals infiltrate and deposit within their matrix framework. Thus, the original microstructure of the hydrogel controlled their final morphologies after mineralization and resulted in high mineral content. Because the ability to engineer specific peptide sequences derived from elastin allows the precise control of the physicochemical and structural characteristics of the recombinamers, i.e., mechanical stability, elasticity, inherent bioactivity, and self-assembly properties,[31] this expands the potential applications of ELRs, in particular their biomineralization and use in hard-tissue regeneration.

2. MATERIALS AND METHODS

2.1. Materials. ELRs HSS_3 and REDV were synthesized according to the published procedures,[32] and their physicochemical properties are listed in Table 1. Sequences of the two ELRs are as follows: HSS_3: [((VPGIG)$_2$VPGKG(VPGIG)$_2$)DDDEEKFLRRIGRFG-((VPGIG)$_2$VPGKG(VPGIG)$_2$)]$_3$(VPAVG)$_{20}$[((VPGIG)$_2$VPGKG-(VPGIG)$_2$)DDDEEKFLRRIGRFG((VPGIG)$_2$VPGKG(VPGIG)$_2$)]$_3$; REDV: [(VPGIG)$_2$(VPGKG)(VPGIG)$_2$EEIQIGHIPREDVDYHLYP-(VPGIG)$_2$(VPGKG)(VPGIG)$_2$(VGVAPG)$_3$]$_{10}$.

Sodium phosphate dibasic and *N*-hydroxysuccinimide (NHS) were purchased from Fischer Scientific (Pittsburgh, PA, USA). Poly(L-aspartic acid) (polyAsp) sodium salts were purchased from Alamanda Polymers (Huntsville, AL, USA). 1-Ethyl-3-[3-(dimethylamino)-propyl] carbodiimide hydrochloride (EDC) and all other chemicals were purchased from Sigma-Aldrich (St. Louis, MO, USA).

Table 1. Physicochemical Properties of the Elastin-Like Recombinamers[a]

ELR	molecular weight M_w (kDa)	isoelectric point	net charge at pH 7.0	ratio of hydrophilic residues/total number of residues (%)
HSS_3	44.9	10.3	8.0	13
REDV	80.1	5.3	−18.1	10

[a]Peptide calculator: http://www.bachem.com (accessed on October 19, 2015).

2.2. Preparation of Cross-Linked ELR Hydrogels and Mineralization. ELR molecules were cross-linked with EDC and NHS. Briefly, 7 mg of ELRs were dissolved in 1 mL of 2-(N-morpholino) ethanesulfonic acid (MES, 50 mM, pH 6.8) mixed with 50 mM EDC and 25 mM NHS and stored at 4 °C overnight for cross-linking. They were then centrifuged at 37 °C, and the precipitate was immersed in a solution containing 0.1 M Na_2HPO_4 and 2 M NaCl for 2 h to hydrolyze any remaining activated carboxyl groups of peptides and EDC. After rinsing with distilled water, the cross-linked hydrogels were obtained. Mineralization of the cross-linked ELR hydrogel was conducted via the PILP process.[34] Mineralization solution was prepared by mixing equal volumes 9 mM $CaCl_2{\cdot}2H_2O$ and 4.2 mM K_2HPO_4 in Tris-buffered saline (pH 7.4 at 37 °C). polyAsp sodium salt (M_w: 27 000 Da, 50 μg/mL) was dissolved in the $CaCl_2$ solution described above before mixing. Mineralization (7−28 days) was performed because it has been generally used in biomimetic mineralization systems.[35,36] The PILP solution was refreshed every 3 days during the mineralization.

2.3. Characterization of the Mineralized Hydrogels. Differential scanning calorimetry (DSC, TA Instruments Q1000, USA) was used to analyze the thermal response of HSS_3. A 10 μL aliquot of a 50 mg/mL HSS_3 aqueous solution was placed in a 20 μL aluminum pan and sealed. An equal volume of distilled water was placed in a reference pan. They were heated from 0 to 40 °C at a constant rate of 5 °C per min to obtain isothermal curves. The morphologies of the hydrogels before and after mineralization were analyzed by FE-SEM (JEOL 6500, Tokyo, Japan) at 5 kV and FE-TEM (FEI Tecnai G2 F30, Hillsboro, OR, USA) at 300 kV. For SEM, the samples were lyophilized and sputter-coated with 5 nm of Pt. Energy dispersive X-ray spectroscopy (EDS) analysis was performed during SEM analysis at 15 kV. TEM samples were prepared by embedding the lyophilized sample in epoxy resin, cut with an ultramicrotome (Leica Reichert UltraCut S) at room temperature, and collected on copper grids. Selected-area electron diffraction (SAED) was performed during TEM analysis to identify the crystallinity of the minerals. The crystal structure of the minerals was also characterized using a micro-diffractometric system with a 2D area detector (Bruker AXS, Germany) at 45 kV and 40 mA. The incident angle was 15°, and the detector position was fixed at 30°, which covered the angular range from 15 to 45° in 2θ. Data collection time was 1000s, and the results were analyzed using the JADE8 software (Materials Data Inc., JADE, Livermore, CA, USA). Microcomputed tomography (μ-CT, HMX-XT 225, X-tek system, United Kingdom) was used to determine 3D structure and mineral density of the hydrogel after mineralization using the following operational parameters: 90 kV, 90 μA, 720 projections, and 4 frames per projection. The volumetric reconstruction of the microradiographs was performed using CT Pro 3D (Nikon Metrology, Brighton, MI, USA); then, the reconstructed volume was analyzed using VG Studio Max (Version 2.1.3, 64 bit, Volume Graphics, Charlotte, NC, USA). An HSS_3 hydrogel after 28 days of mineralization (approximately 0.4 × 1.5 × 1.5 cm^3) as well as a bovine dentin and cortical bone block were used for this analysis. Mineral density was quantified by comparing the attenuation coefficient of the mineralized hydrogel with CT-based calibration phantoms of HA.

DOI: 10.1021/acsami.5b07628
ACS Appl. Mater. Interfaces XXXX, XXX, XXX−XXX

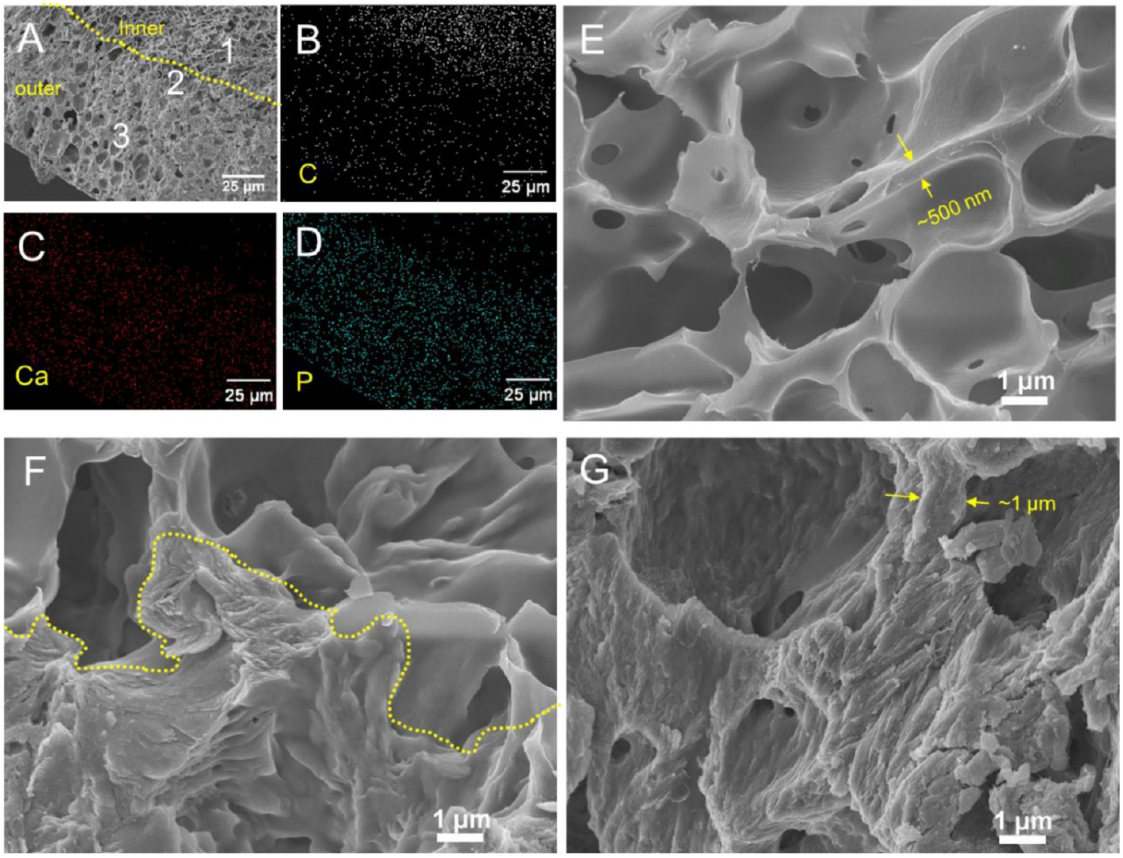

Figure 1. (A–D) Cross-sectional SEM image and elemental mapping of the cross-linked HSS_3 hydrogel after 14 days of mineralization in the PILP solution. (E–G) Cross-sectional SEM images from the regions of 1, 2, and 3 marked in A, respectively. The dashed lines indicate the interface between the outer mineralized and the inner nonmineralized regions.

2.4. Mechanical Testing. Mechanical properties of the ELR hydrogel after 28 days of mineralization were examined by nanoindentation using a MTS nanoindenter XP, equipped with a Berkovich tip at room temperature. Testworks 4 software, which incorporates the Oliver–Pharr data analysis method[37] was used to analyze their elastic modulus and hardness. Ultramicrotome sectioning was used to reveal the indentation surfaces of the mineralized region of the hydrogel that was embedded in an epoxy resin. Nanoindentation was also performed on a cortical bone from bovine tibia. Preparation of bone sample was performed as we previously described.[34] Briefly, bovine cortical bone was embeded into PMMA, sectioned with a low-speed diamond saw (Isomet, Buehler, Lake Bluff, IL, USA), ground with sand papers (SiC, 600, 1000, and 1200), and polished with alumina suspensions (5 , 1, and 0.1 μm) to obain a smooth surface suitable for nanoindentation. A total of 10 indents were performed on each sample. Mean elastic modulus and hardness were obtained from representative properties–displacement curves at a depth of 2000 μm.

2.5. Statistical Analysis. Analysis of the statistically significant differences on mechanical properties among groups was performed with one-way ANOVA tables (SPSS v.19, IBM). The level of statistical significance was set at $p < 0.05$.

3. RESULTS AND DISCUSSION

3.1. Thermoresponsive Behavior of HSS_3. HSS_3 used in this study is an ABA amphiphilic triblock ELR. Block A is composed of $[[(VPGIG)_2(VPGKG)(VPGIG)_2]_2DDDEEKFLRRIGRFG[(VPGIG)_2(VPGKG)(VPGIG)_2]_2]_3$. Block B is $(VPAVG)_{20}$. This block polymer displays the aforementioned reverse thermal response. DSC analysis revealed its endotherm ranged from 22 to 37 °C, which was resolved in two peaks corresponding to the individual transitions of the hydrophobic moieties of the two different blocks (Figure S1). Although the hydrophobic moieties of both blocks have similar polarity, the influence of the nearby polar amino acids might shift the T_t of the block A to a value higher than that of the block B.[38]

3.2. Fabrication and Mineralization of Cross-Linked HSS_3 Hydrogels. When the HSS_3 molecules were cross-linked with carbodiimides, they formed microporous hydrogels (Figure S2). These hydrogels were transparent at 4 °C. They became opaque rapidly when incubated at 37 °C, indicating the occurrence of phase transition. Mineralization via the PILP process using 50 μg/mL polyaspartate (M_w: 27 000 Da) as process-directing agent was conducted, and the PILP solution was replaced every 3 days to keep it clear. After 14 days of mineralization, mineralization depth of 78 ± 4 μm was achieved on the outer region of the porous HSS_3 hydrogel showing strong signals of calcium and phosphate, whereas a large amount of carbon along with sparse signals of calcium and phosphate were found in its inner side (Figure 1). The thickness of the hydrogel framework at the nonmineralized region was around 500 nm (Figure 1E), and it was approximately 1 μm at the mineralized region (Figure 1G). In contrast to the conventional mineralization of hydrogels, where HA was precipitated on the surface of the organic matrices,[16,39] the minerals were specifically deposited within the framework of the HSS_3 hydrogel, preserving its microporous structure. Besides, the texture of the mineralized region showed striking similarity to that of the cortical bone at the nanoscale (Figure S3).

DOI: 10.1021/acsami.5b07628
ACS Appl. Mater. Interfaces XXXX, XXX, XXX–XXX

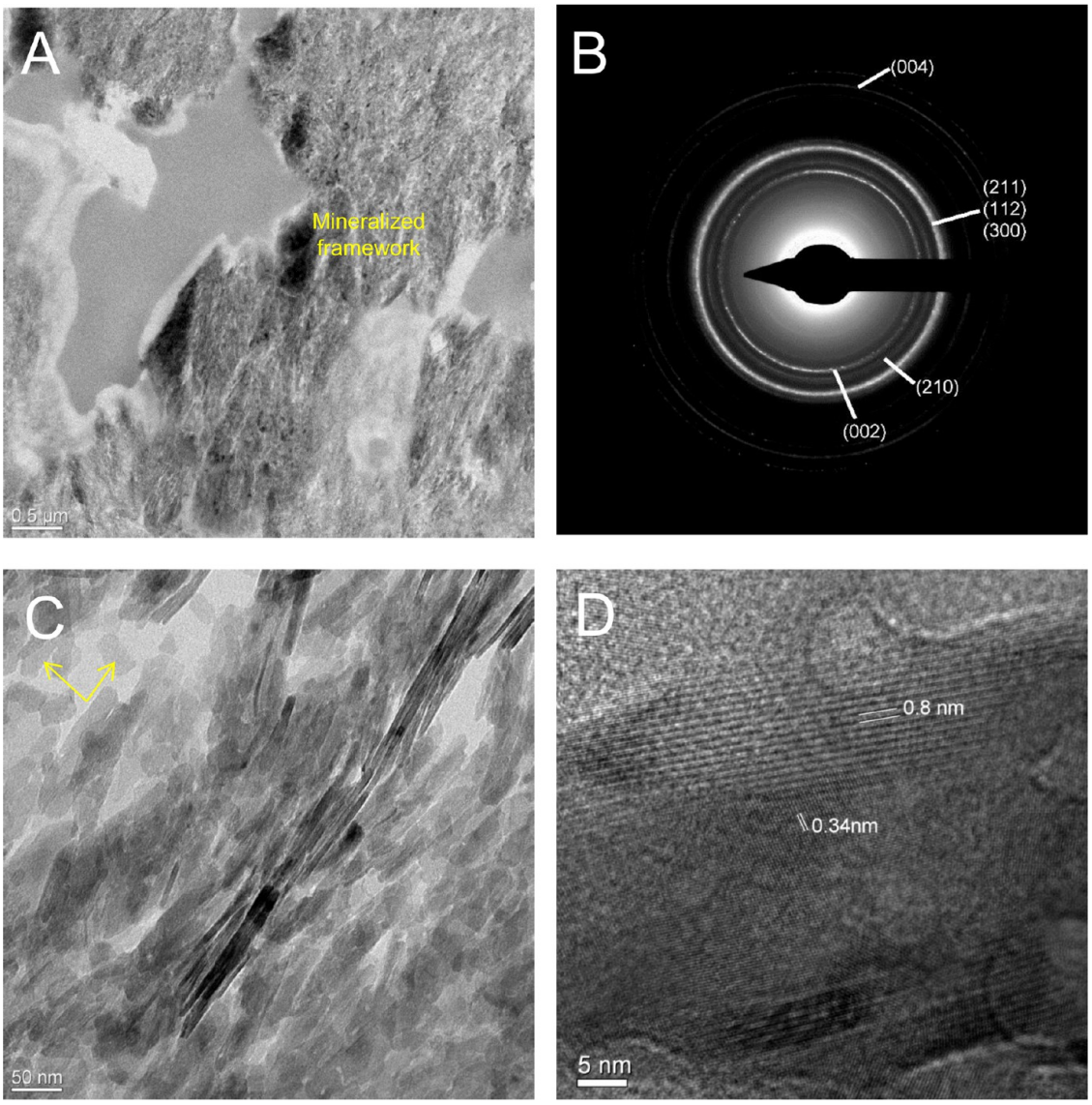

Figure 2. TEM images of the cross-linked HSS_3 hydrogel after 14 days of mineralization. (A) Representative TEM image and (B) corresponding SAED pattern of the hydrogel at the mineralized region. The minerals were homogeneously distributed in the framework of the hydrogel, and they were randomly oriented HA nanocrystals. (C) Hydroxyapatite nanocrystals were needlelike. Platelike fragments (pointed to by arrows) without lattice fringes were presumably from the organic hydrogel. (D) HR-TEM lattice image of HA nanocrystals showing 0.8 and 0.34 nm planar spacing, which correspond to the HA (100) and (002) planes, respectively.

TEM images revealed that nanocrystals were homogeneously deposited in the hydrogel framework at the mineralized region (Figure 2A). SAED produced a multiple-ring-shaped diffraction pattern for HA, including a ring for the (002) and (210) planes and one for the combined (211), (112), and (300) planes (Figure 2B), indicating that the crystals were randomly oriented in the hydrogel framework. Such crystal orientation is different from the one found in mineralized collagen fibrils where the nanocrystals were oriented parallel to the longitudinal axes of the collagen fibrils. Because the polymer chains in the hydrogel framework were randomly distributed, it may not contain oriented confinements to guide the crystal orientation that found in the collagen system.[40,41] The crystals were needlelike, approximately 10 nm wide and 50−150 nm long (Figure 2C). They had 0.8 and 0.34 nm planar spacings as assessed with the HR-TEM lattice image (Figure 2D), which correspond to the (100) and (002) planes of HA, respectively. X-ray diffraction spectra further confirmed that the minerals were HA nanocrystals (Figure 3). Peaks for the (002), (210), (211), (202), and (310) planes of HA were broad and matched well with the diffraction pattern of bovine cortical bone.

3.3. The Role of Elastin-Like Recombinamers on Mineralization. Unlike in classical crystal nucleation, where nucleation from a supersaturated solution occurs when a sufficiently large density fluctuation of the solution overcomes a free energy barrier between the crystalline and solution phases, calcium phosphate biomineralization proceeds via an amorphous precursor phase.[8,42] The PILP process is a biomimetic mineralization system in which anionic polyaspartic acids mimic the role of acidic proteins in biominerals, forming a liquidlike ACP precursor complex.[4] Because of its fluidlike characteristics, the PILP process does not require specific interactions with specific crystallographic planes in contrast to the classical crystallization.[22] These liquid precursors are well-suited to achieve the controlled morphogenesis using templates because they can easily adapt to any shape before crystallization.[20] They

DOI: 10.1021/acsami.5b07628
ACS Appl. Mater. Interfaces XXXX, XXX, XXX−XXX

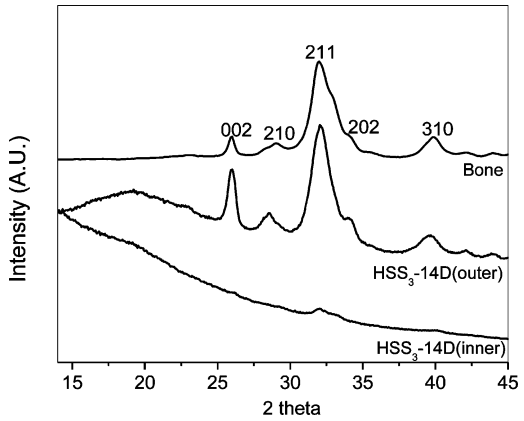

Figure 3. XRD spectra of the cross-linked HSS_3 hydrogel after 14 days of mineralization in the inner nonmineralized and outer mineralized regions as well as bovine cortical bone.

can even infiltrate into small cavities of the insoluble organic matrix as found in the bone and dentin; i.e., the ACP nanoclusters deposit into the gap zones and nanochannels of the type-I collagen fibrils.[3,4,12]

It has been demonstrated that elastin-like poly(VPGVG) and its analogs poly[f_v(VPGVG), f_x(VPGKG)] ($0.1 \leq f_x \leq 0.2$, $f_v + f_x = 1$) undergo hierarchical self-assembly.[43] At the nanoscale, those ELRs self-assembled into 5 nm wide twisted filaments consisting of several β spirals. These filaments were aligned in parallel into fibrils several hundred nanometers in diameter. The HSS_3 molecules in aqueous solution can also self-assemble into anisotropic fibrils around 150 nm in diameter at 37 °C (Figure S4). Although the HSS_3 chains in the hydrogel were cross-linked, the ordered structures, such as β spiral and twisted filament may still form at a temperature above T_t because the hydrogel exhibited opalescence, an indication of microphase separation (microdomains in tens of nanometers) between hydrophobic and hydrophilic moieties.[31,44] Therefore, nanopores and/or nanochannels from the hydrophilic moieties may form within the hydrogel framework, serving as compartments for mineral deposition. It is possible that the amorphous precursor nanoclusters infiltrate into the nanocompartments of the ELR hydrogel and then coalesce, solidify, and crystallize to form close-packed crystals. Further investigations on the mechanisms of mineralization in the ELR hydrogels are underway.

The peptide sequence of SN_A15 (DDDEEKFLRRIGRFG), derived from statherin, may promote the uptake of the liquid ACP precursor into the hydrogel. Statherin is an acidic phosphopeptide with a high degree of structural and charge asymmetry.[45] SN_A15 has a high binding affinity and crystal growth inhibition to calcium phosphate minerals.[46] Previously, we have demonstrated that statherin-derived ELRs have the ability to induce and control the growth of minerals on biofunctionalized surfaces.[47] However, the sequence of SN_A15 may not be critical for mineral infiltration. As shown in Figure f4

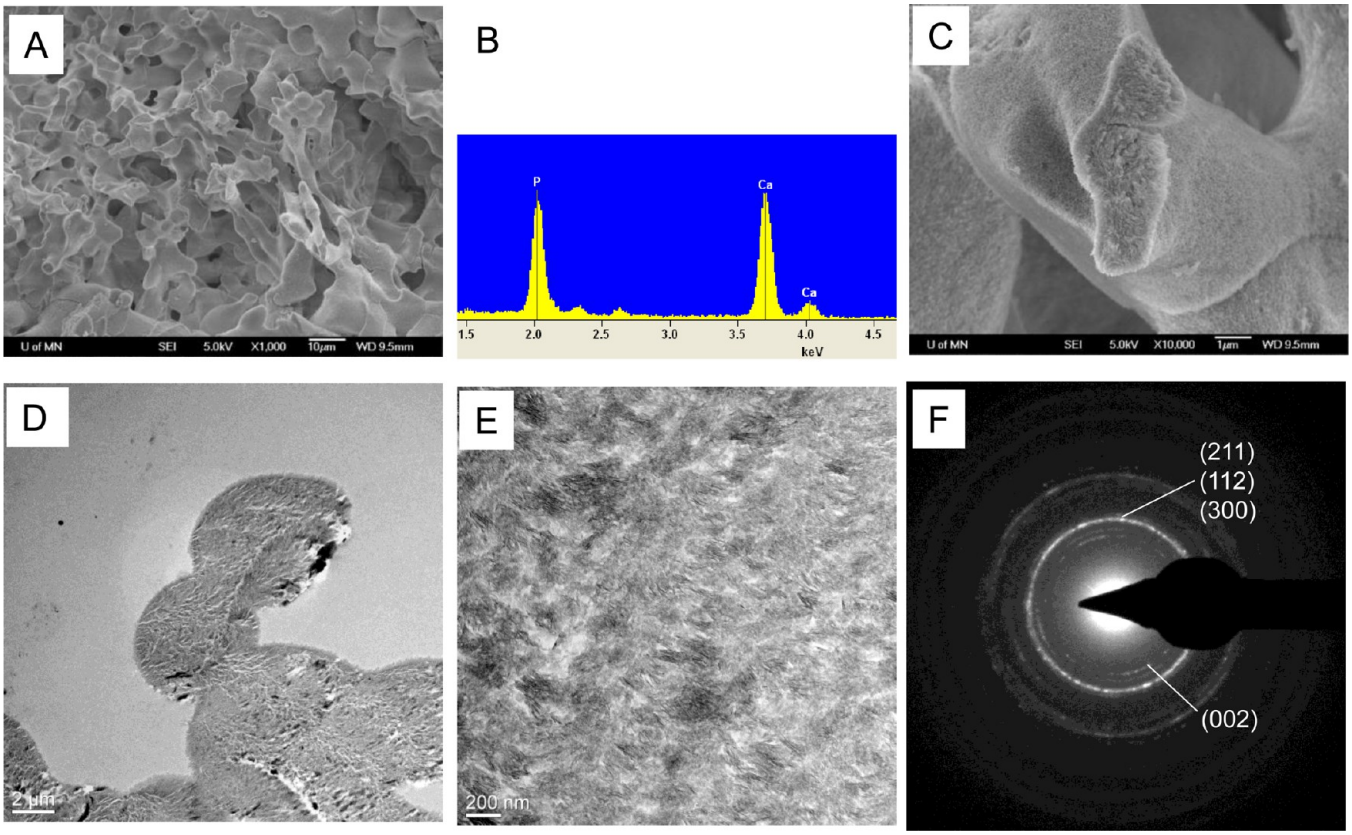

Figure 4. SEM and TEM analysis of the REDV hydrogel after 14 days of mineralization by the PILP process. (A) SEM image and (B) its corresponding EDS of the mineralized REDV, showing that calcium phosphate minerals were deposited into the REDV hydrogel framework. (C) Fractured surface of the REDV hydrogel after mineralization. (D) TEM image of the mineralized REDV hydrogel showing densely packed and homogeneously distributed minerals in the polymeric matrix. (E and F) TEM image and the corresponding SAED pattern, respectively, revealed that the randomly oriented minerals were needlelike HA nanocrystals.

DOI: 10.1021/acsami.5b07628
ACS Appl. Mater. Interfaces XXXX, XXX, XXX−XXX

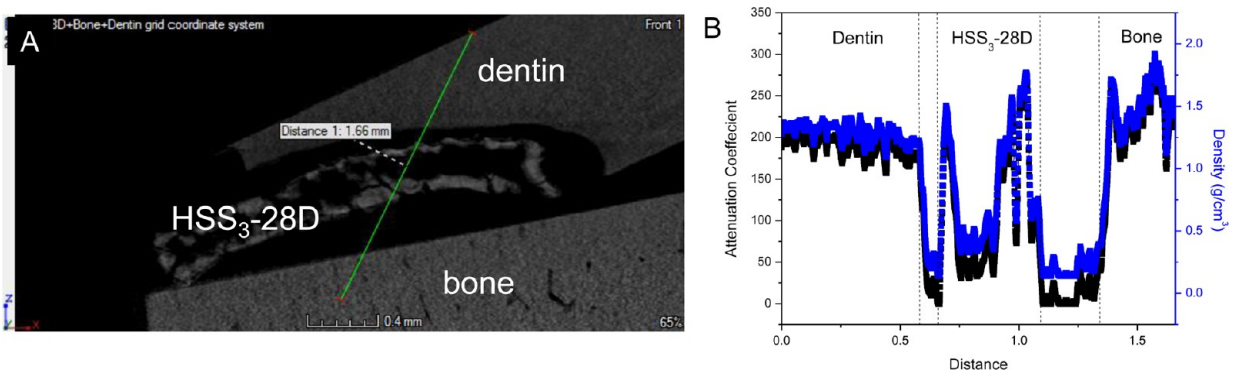

Figure 5. (A) Micro-CT image of dentin, bone, and the HSS_3 hydrogel after 28 days of mineralization (HSS_3-28D). (B) Distribution of the attenuation coefficient and mineral density of the region marked with a green line in A.

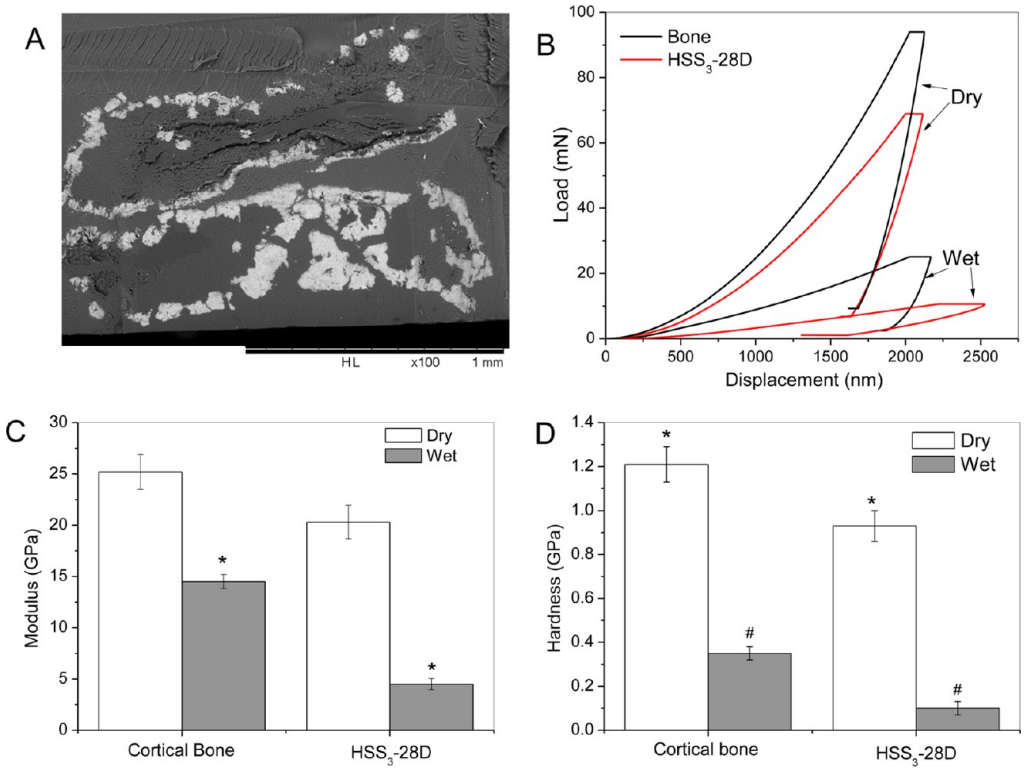

Figure 6. (A) SEM image of the microtome section of HSS_3-28D used for nanoindentation. Representative (B) nanoindentation load−displacement curves, (C) elastic modulus, and (D) hardness of the bovine cortical bone and the HSS_3-28D in the dry and wet states.

4, the REDV hydrogel contains no SN_A15 and was also successfully mineralized. After 14 days of mineralization, the framework of the cross-linked REDV hydrogel was still discernible (Figure 4A), and the corresponding EDS analysis confirmed the presence of calcium and phosphate (Figure 4B). The fractured surface of the mineralized REDV showed a homogeneously granular morphology, indicating that the minerals have deposited within the framework and were well-integrated with the organic REDV hydrogel (Figure 4C). TEM (Figure 4D,E) and SAED (Figure 4F) images demonstrated that needlelike HA nanocrystals were randomly distributed in the REDV hydrogel, similar to those found in the mineralized HSS_3 hydrogel (Figure 2). Previous studies suggested that electrostatic interactions between amorphous ACP clusters and collagen-mediated infiltration of the mineral into the collagen fibrillar matrix, i.e., polyaspartic acid molecules formed negatively charged complexes with ACP that interacted with a positively charged region of collagen located at the C-terminal region of the gap zone.[4] Our results demonstrated that ACP nanoclusters can infiltrate into negatively charged REDV matrices (Table 1), suggesting that the electrostatic interactions may not be the major driving force for the mineralization in these organic matrix frameworks.

3.3. Mineral Density and Nanoindentation. Micro-CT analysis of the HSS_3 hydrogel after 28 days of mineralization demonstrated that a mineral density of up to 1.90 $g \cdot cm^{-3}$ was achieved, which is higher than that of dentin but lower than that of bovine cortical bone (Figure 5A,B).

Mechanical properties of the hydrogel at the mineralized region were measured by nanoindentation and compared to those of bovine cortical bone. As shown in Figure 6A, the thickness of the mineralized region ranged from 40−200 μm. In the dry state, the load−displacement curve (Figure 6B) was remarkably similar to the one obtained from bovine cortical

DOI: 10.1021/acsami.5b07628
ACS Appl. Mater. Interfaces XXXX, XXX, XXX−XXX

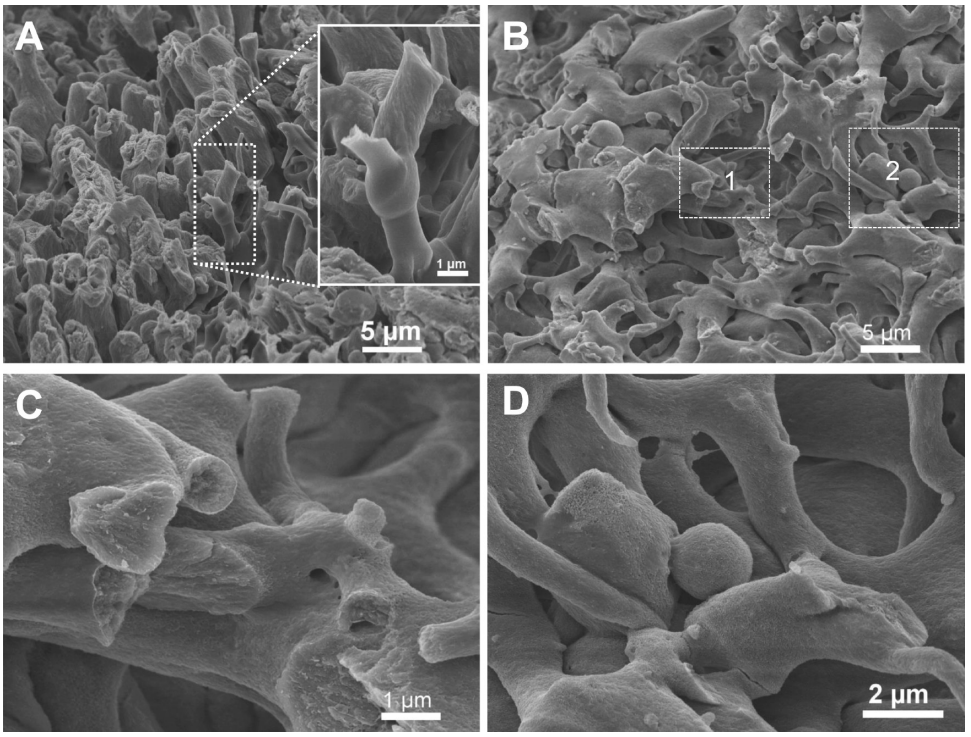

Figure 7. SEM images of the cross-linked HSS_3 hydrogel after 7 days of mineralization. (A) Fractured framework of the hydrogel. Insert: a hydrogel strut that displayed mineralized top and unmineralized bottom. (B) Complex interwoven network of struts and microspheres with granular surfaces. (C and D) Higher-magnification SEM images of the fractured surface of the hydrogel framework from areas 1 and 2 marked in B, which are indicative of the full integration between the minerals and the HSS_3 matrices.

bone. Its elastic modulus was 20.3 ± 1.7 GPa, comparable to natural cortical bone, whereas its hardness (0.93 ± 0.07 GPa) was significantly lower than that of bone (Figure 6C,D). When the specimen was hydrated, the mechanical properties of both the mineralized hydrogel and cortical bone were significantly reduced. The elastic modulus and hardness of mineralized hydrogel were decreased to 4.50 ± 0.55 and 0.10 ± 0.03 GPa, respectively. In the wet state, the mechanical properties of the mineralized region of the hydrogel were significantly lower, around one-third of those measured for bovine cortical bone. It has been reported that the elastic modulus of demineralized dentin lesions can be restored from 0.2 GPa to near 10 GPa in a wet state after 14 days of mineralization using the PILP process.[56] Our previous study also demonstrated that the hardness and elastic modulus of the nanoporous intrafibrillarly mineralized collagen films were 0.7 and 9.1 GPa, respectively, in the dry state, whereas in the wet state they were 9 and 177 MPa, respectively.[34] In contrast, the mechanical properties of the mineralized ELRs studied here were over 1 order of magnitude higher than those of the nanoporous intrafibrillarly mineralized collagen films and on the same order of magnitude as those of the restored dentin lesions.

3.4. ELR-Template-Directed Control of Hybrid Morphologies. The use of insoluble organic matrices as a morphological template for the bottom-up fabrication of organic−inorganic nanocomposites is a powerful way to build a variety of advanced hybrid biomaterials. In contrast to metals and ceramics, polymers are much more easily fabricated into diverse shapes. By controlling mineral deposition in the organic matrices, predictable morphology of the nanocomposites can be obtained. In our study, many struts were observed on a HSS_3 hydrogel after mineralization (Figure 7A). In some cases, they showed a granular/rough surface (top part in inset of Figure 7A) or a smooth surface (bottom part, inset of Figure 7A), revealing the occurrence of ongoing mineralization. Interwoven struts and microspheres with fully granular surfaces were also found (Figure 7B−D). These complex morphologies and shapes with curved surfaces suggested that the original microstructure of the hydrogel dictated the final morphology of the nanocomposites.

CONCLUSIONS

We have demonstrated that hydrogels of the elastin-like recombinamers templated calcium phosphate mineralization where the minerals selectively deposited within the hydrogel frameworks. By using a bottom-up method, a new class of hybrid nanocomposites with controlled morphologies was developed. These composites possessed microporous structures and mineral density comparable to that of natural bone. Their mechanical properties were on the same order of magnitude as those measured from bovine cortical bone. The use of the ELR hydrogels opens the possibility to study in vitro model systems that reproduce biomimetic processes. By designing the sequence of the ELRs and controlling the morphologies of ELRs matrices at different dimensional levels, diverse hybrid nanocomposites with optimized mechanical and biological properties can be constructed and can be suited for the treatment of bone defects using regenerative medicine approaches.

ASSOCIATED CONTENT

Supporting Information

The Supporting Information is available free of charge on the ACS Publications website at DOI: 10.1021/acsami.5b07628.

DOI: 10.1021/acsami.5b07628
ACS Appl. Mater. Interfaces XXXX, XXX, XXX−XXX

DSC analysis on phase transition of HSS_3 in an aqueous solution, SEM visualization of the porous HSS_3 hydrogels, SEM comparative images of the mineralized scaffolds and cortical bone, and the self-assembled fibrillar structures of HSS_3. (PDF)

AUTHOR INFORMATION

Corresponding Authors

*E-mail: apari003@umn.edu.

*E-mail: lixx1191@umn.edu. Tel.: +1-612-625-4467. Fax: +1-612-626-1484.

Notes

The authors declare no competing financial interest.

ACKNOWLEDGMENTS

This project was partially supported by a 3M Foundation Non-Tenured Faculty Award to C.A.. J.C.R.-C. wishes to thank The European Commission under FP7 and H2020 programs (NMP3-LA-2011-263363; HEALTH-F4-2011-278557; PITN-GA-2012-317304; MSCA-ITN-2014-ETN- 642687; and H2020-NMP-2014- 646075), The Ministry of Economy and Competitiveness (Spain) (MAT2012-38043-C02-01; MAT2013−41723-R; and MAT2013−42473-R), and the Junta de Castilla y Leon (VA244U13; VA313U14). X.C. would like to thank the National Institute for Dental and Craniofacial Research (NIDCR) of the U.S. National Institutes of Health for fellowship support through the training grant R90DE023058. Parts of this work were carried out in the University of Minnesota I.T. Characterization Facility, which receives partial support from NSF through the MRSEC program.

REFERENCES

(1) Weiner, S.; Wagner, H. D. The Material Bone: Structure Mechanical Function Relations. *Annu. Rev. Mater. Sci.* **1998**, *28*, 271−298.

(2) Fratzl, P.; Gupta, H. S.; Paschalis, E. P.; Roschger, P. Structure and Mechanical Quality of the Collagen-Mineral Nano-Composite in Bone. *J. Mater. Chem.* **2004**, *14* (14), 2115−2123.

(3) Olszta, M. J.; Cheng, X. G.; Jee, S. S.; Kumar, R.; Kim, Y. Y.; Kaufman, M. J.; Douglas, E. P.; Gower, L. B. Bone Structure and Formation: A New Perspective. *Mater. Sci. Eng., R* **2007**, *58* (3−5), 77−116.

(4) Nudelman, F.; Pieterse, K.; George, A.; Bomans, P. H. H.; Friedrich, H.; Brylka, L. J.; Hilbers, P. A. J.; de With, G.; Sommerdijk, N. A. J. M. The Role of Collagen in Bone Apatite Formation in the Presence of Hydroxyapatite Nucleation Inhibitors. *Nat. Mater.* **2010**, *9* (12), 1004−1009.

(5) Hunter, G. K.; Goldberg, H. A. Modulation of Crystal-Formation by Bone Phosphoproteins - Role of Glutamic Acid-Rich Sequences in the Nucleation of Hydroxyapatite by Bone Sialoprotein. *Biochem. J.* **1994**, *302*, 175−179.

(6) George, A.; Bannon, L.; Sabsay, B.; Dillon, J. W.; Malone, J.; Veis, A.; Jenkins, N. A.; Gilbert, D. J.; Copeland, N. G. The Carboxyl-Terminal Domain of Phosphophoryn Contains Unique Extended Triplet Amino Acid Repeat Sequences Forming Ordered Carboxyl-Phosphate Interaction Ridges That may be Essential in the Biomineralization Process. *J. Biol. Chem.* **1996**, *271* (51), 32869−32873.

(7) Schwartz, S. S.; Hay, D. I.; Schluckebier, S. K. Inhibition of Calcium-Phosphate Precipitation by Human Salivary Statherin - Structure-Activity-Relationships. *Calcif. Tissue Int.* **1992**, *50* (6), 511−517.

(8) Mahamid, J.; Sharir, A.; Addadi, L.; Weiner, S. Amorphous Calcium Phosphate is a Major Component of the Forming Fin Bones of Zebrafish: Indications for an Amorphous Precursor Phase. *Proc. Natl. Acad. Sci. U. S. A.* **2008**, *105* (35), 12748−12753.

(9) Traub, W.; Arad, T.; Weiner, S. 3-Dimensional Ordered Distribution of Crystals in Turkey Tendon Collagen-Fibers. *Proc. Natl. Acad. Sci. U. S. A.* **1989**, *86* (24), 9822−9826.

(10) Landis, W. J.; Hodgens, K. J.; Arena, J.; Song, M. J.; McEwen, B. F. Structural Relations between Collagen and Mineral in Bone as Determined by High Voltage Electron Microscopic Tomography. *Microsc. Res. Tech.* **1996**, *33* (2), 192−202.

(11) Abraham, Y.; Tamburu, C.; Klein, E.; Dunlop, J. W. C.; Fratzl, P.; Raviv, U.; Elbaum, R. Tilted Cellulose Arrangement as a Novel Mechanism for Hygroscopic Coiling in the Stork's Bill Awn. *J. R. Soc., Interface* **2012**, *9* (69), 640−647.

(12) Li, Y. P.; Aparicio, C. Discerning the Subfibrillar Structure of Mineralized Collagen Fibrils: A Model for the Ultrastructure of Bone. *PLoS One* **2013**, *8* (9), e76782.

(13) Phadke, A.; Zhang, C.; Hwang, Y.; Vecchio, K.; Varghese, S. Templated Mineralization of Synthetic Hydrogels for Bone-Like Composite Materials: Role of Matrix Hydrophobicity. *Biomacromolecules* **2010**, *11* (8), 2060−2068.

(14) Liu, P. S.; Song, J. Sulfobetaine as a Zwitterionic Mediator for 3D Hydroxyapatite Mineralization. *Biomaterials* **2013**, *34* (10), 2442−2454.

(15) Junginger, M.; Kita-Tokarczyk, K.; Schuster, T.; Reiche, J.; Schacher, F.; Muller, A. H. E.; Colfen, H.; Taubert, A. Calcium Phosphate Mineralization beneath a Polycationic Monolayer at the Air-Water Interface. *Macromol. Biosci.* **2010**, *10* (9), 1084−1092.

(16) Zhang, R. Y.; Ma, P. X. Biomimetic Polymer/Apatite Composite Scaffolds for Mineralized Tissue Engineering. *Macromol. Biosci.* **2004**, *4* (2), 100−111.

(17) Song, J.; Saiz, E.; Bertozzi, C. R. A New Approach to Mineralization of Biocompatible Hydrogel Scaffolds: an Efficient Process toward 3-Dimensional Bonelike Composites. *J. Am. Chem. Soc.* **2003**, *125* (5), 1236−1243.

(18) Chen, P. Y.; Toroian, D.; Price, P. A.; McKittrick, J. Minerals Form a Continuum Phase in Mature Cancellous Bone. *Calcif. Tissue Int.* **2011**, *88* (5), 351−361.

(19) Gower, L. B. Biomimetic Model Systems for Investigating the Amorphous Precursor Pathway and Its Role in Biomineralization. *Chem. Rev.* **2008**, *108* (11), 4551−4627.

(20) Meldrum, F. C.; Colfen, H. Controlling Mineral Morphologies and Structures in Biological and Synthetic Systems. *Chem. Rev.* **2008**, *108* (11), 4332−4432.

(21) Politi, Y.; Arad, T.; Klein, E.; Weiner, S.; Addadi, L. Sea Urchin Spine Calcite Forms via a Transient Amorphous Calcium Carbonate Phase. *Science* **2004**, *306* (5699), 1161−1164.

(22) Cheng, X. G.; Gower, L. B. Molding Mineral Within Microporous Hydrogels by a Polymer-Induced Liquid-Precursor (PILP) Process. *Biotechnol. Prog.* **2006**, *22* (1), 141−149.

(23) Meldrum, F. C.; Ludwigs, S. Template-Directed Control of Crystal Morphologies. *Macromol. Biosci.* **2007**, *7* (2), 152−162.

(24) Gotliv, B. A.; Addadi, L.; Weiner, S. Mollusk Shell Acidic Proteins: In Search of Individual Functions. *ChemBioChem* **2003**, *4* (6), 522−529.

(25) Falini, G.; Albeck, S.; Weiner, S.; Addadi, L. Control of Aragonite or Calcite Polymorphism by Mollusk Shell Macromolecules. *Science* **1996**, *271* (5245), 67−69.

(26) Faury, G. Function-Structure Relationship of Elastic Arteries in Evolution: from Microfibrils to Elastin and Elastic Fibres. *Pathol. Biol.* **2001**, *49* (4), 310−325.

(27) Martyn, C. N.; Greenwald, S. E. A Hypothesis about a Mechanism for the Programming of Blood Pressure and Vascular Disease in Early Life. *Clin. Exp. Pharmacol. Physiol.* **2001**, *28* (11), 948−951.

(28) Arias, F. J.; Reboto, V.; Martin, S.; Lopez, I.; Rodriguez-Cabello, J. C. Tailored Recombinant Elastin-Like Polymers for Advanced Biomedical and Nano(Bio)Technological Applications. *Biotechnol. Lett.* **2006**, *28* (10), 687−695.

DOI: 10.1021/acsami.5b07628
ACS Appl. Mater. Interfaces XXXX, XXX, XXX−XXX

(29) Urry, D. W. Molecular Machines - How Motion and Other Functions of Living Organisms Can Result from Reversible Chemical-Changes. *Angew. Chem., Int. Ed. Engl.* **1993**, *32* (6), 819−841.
(30) Prieto, S.; Shkilnyy, A.; Rumplasch, C.; Ribeiro, A.; Arias, F. J.; Rodriguez-Cabello, J. C.; Taubert, A. Biomimetic Calcium Phosphate Mineralization with Multifunctional Elastin-Like Recombinamers. *Biomacromolecules* **2011**, *12* (5), 1480−1486.
(31) Yeo, G. C.; Aghaei-Ghareh-Bolagh, B.; Brackenreg, E. P.; Hiob, M. A.; Lee, P.; Weiss, A. S. Fabricated Elastin *Adv. Healthcare Mater.* **2015**, DOI: 10.1002/adhm.201400781.
(32) Girotti, A.; Reguera, J.; Rodriguez-Cabello, J. C.; Arias, F. J.; Alonso, M.; Testera, A. M. Design and Bioproduction of a Recombinant Multi(bio)functional Elastin-Like Protein Polymer Containing Cell Adhesion Sequences for Tissue Engineering Purposes. *J. Mater. Sci.: Mater. Med.* **2004**, *15* (4), 479−484.
(33) Martin, L.; Alonso, M.; Girotti, A.; Arias, F. J.; Rodriguez-Cabello, J. C. Synthesis and Characterization of Macroporous Thermosensitive Hydrogels from Recombinant Elastin-Like Polymers. *Biomacromolecules* **2009**, *10* (11), 3015−3022.
(34) Li, Y. P.; Thula, T. T.; Jee, S.; Perkins, S. L.; Aparicio, C.; Douglas, E. P.; Gower, L. B. Biomimetic Mineralization of Woven Bone-Like Nanocomposites: Role of Collagen Cross-Links. *Biomacromolecules* **2012**, *13* (1), 49−59.
(35) Bushell, K. N.; Leeman, S. E.; Gillespie, E.; Gower, A. C.; Reed, K. L.; Stucchi, A. F.; Becker, J. M.; Amar, S. LITAF Mediation of Increased TNF-alpha Secretion from Inflamed Colonic Lamina Propria Macrophages. *PLoS One* **2011**, *6* (9), e25849.
(36) Thula, T. T.; Rodriguez, D. E.; Lee, M. H.; Pendi, L.; Podschun, J.; Gower, L. B. In vitro Mineralization of Dense Collagen Substrates: a Biomimetic Approach toward the Development of Bone-Graft Materials. *Acta Biomater.* **2011**, *7* (8), 3158−3169.
(37) Oliver, W. C.; Pharr, G. M. An Improved Technique for Determining Hardness and Elastic-Modulus Using Load and Displacement Sensing Indentation Experiments. *J. Mater. Res.* **1992**, *7* (6), 1564−1583.
(38) Ribeiro, A.; Arias, F. J.; Reguera, J.; Alonso, M.; Rodriguez-Cabello, J. C. Influence of the Amino-Acid Sequence on the Inverse Temperature Transition of Elastin-Like Polymers. *Biophys. J.* **2009**, *97* (1), 312−320.
(39) Jee, S. S.; Culver, L.; Li, Y. P.; Douglas, E. P.; Gower, L. B. Biomimetic Mineralization of Collagen via an Enzyme-Aided PILP Process. *J. Cryst. Growth* **2010**, *312* (8), 1249−1256.
(40) He, W. X.; Rajasekharan, A. K.; Tehrani-Bagha, A. R.; Andersson, M. Mesoscopically Ordered Bone-Mimetic Nanocomposites. *Adv. Mater.* **2015**, *27* (13), 2260−2264.
(41) Cantaert, B.; Beniash, E.; Meldrum, F. C. Nanoscale Confinement Controls the Crystallization of Calcium Phosphate: Relevance to Bone Formation. *Chem. - Eur. J.* **2013**, *19* (44), 14918−14924.
(42) Mahamid, J.; Aichmayer, B.; Shimoni, E.; Ziblat, R.; Li, C. H.; Siegel, S.; Paris, O.; Fratzl, P.; Weiner, S.; Addadi, L. Mapping Amorphous Calcium Phosphate Transformation into Crystalline Mineral from the Cell to the Bone in Zebrafish Fin Rays. *Proc. Natl. Acad. Sci. U. S. A.* **2010**, *107* (14), 6316−6321.
(43) Urry, D. W.; Okamoto, K.; Harris, R. D.; Hendrix, C. F.; Long, M. M. Synthetic, Cross-Linked Polypentapeptide of Tropoelastin - Anisotropic, Fibrillar Elastomer. *Biochemistry* **1976**, *15* (18), 4083−4089.
(44) Du, A.; Zhou, B.; Xu, W. W.; Yu, Q. J.; Shen, Y.; Zhang, Z. H.; Shen, J.; Wu, G. M. Reaction-Induced Microsyneresis in Oxide-Based Gels: The Assembly of Hierarchical Microsphere Networks. *Langmuir* **2013**, *29* (36), 11208−11216.
(45) Wojciechowska, I.; Kochanska, B.; Stelmanska, E.; Knap, N.; Mackiewicz, Z.; Kupryszewski, G. Statherin and its Shortened Analogues. *Polish J. Chem.* **1998**, *72* (9), 2098−2102.
(46) Raj, P. A.; Johnsson, M.; Levine, M. J.; Nancollas, G. H. Salivary Statherin - Dependence on Sequence, Charge, Hydrogen-Bonding Potency, and Helical Conformation for Adsorption to Hydroxyapatite and Inhibition of Mineralization. *J. Biol. Chem.* **1992**, *267* (9), 5968−5976.
(47) Li, Y. P.; Chen, X.; Ribeiro, A. J.; Jensen, E. D.; Holmberg, K. V.; Rodriguez-Cabello, J. C.; Aparicio, C. Hybrid Nanotopographical Surfaces Obtained by Biomimetic Mineralization of Statherin-Inspired Elastin-Like Recombinamers. *Adv. Healthcare Mater.* **2014**, *3* (10), 1638−1647.
(48) Olszta, M. J.; Cheng, X. G.; Jee, S. S.; Kumar, R.; Kim, Y. Y.; Sivakumar, M.; Gower, L.; Douglas, E. P. Organic-Inorganic Composites Mimicking the Nanostructured Architecture of Bone. *Abstr. Pap. Am. Chem. Soc.*, **2006**, *231*.
(49) Liu, Y.; Li, N.; Qi, Y. P.; Dai, L.; Bryan, T. E.; Mao, J.; Pashley, D. H.; Tay, F. R. Intrafibrillar Collagen Mineralization Produced by Biomimetic Hierarchical Nanoapatite Assembly. *Adv. Mater.* **2011**, *23* (8), 975−980.
(50) Wang, Y.; Azais, T.; Robin, M.; Vallee, A.; Catania, C.; Legriel, P.; Pehau-Arnaudet, G.; Babonneau, F.; Giraud-Guille, M. M.; Nassif, N. The Predominant Role of Collagen in the Nucleation, Growth, Structure and Orientation of Bone Apatite. *Nat. Mater.* **2012**, *11* (8), 724−733.
(51) Ferreira, A. M.; Gentile, P.; Chiono, V.; Ciardelli, G. Collagen for Bone Tissue Regeneration. *Acta Biomater.* **2012**, *8* (9), 3191−3200.
(52) Jee, S. S.; Li, Y.; Douglas, E. P.; Gower, L. B. Mimicking the Nanostructure of Bone using a Polymer-Induced Liquid-Precursor (PILP) Mineralization Process. In *A Global Road Map for Ceramic Materials and Technologies: Forecasting the Future of Ceramics, International Ceramic Federation - 2nd International Congress on Ceramics, ICC 2008*, Verona, Italy, June 29−July 4, 2008.
(53) Perez, R. A.; Won, J. E.; Knowles, J. C.; Kim, H. W. Naturally and synthetic Smart Composite Biomaterials for Tissue Regeneration. *Adv. Drug Delivery Rev.* **2013**, *65* (4), 471−496.
(54) Holzwarth, J. M.; Ma, P. X. Biomimetic Nanofibrous Scaffolds for Bone Tissue Engineering. *Biomaterials* **2011**, *32* (36), 9622−9629.
(55) Yang, D. Z.; Jin, Y.; Zhou, Y. S.; Ma, G. P.; Chen, X. M.; Lu, F. M.; Nie, J. In situ Mineralization of Hydroxyapatite on Electrospun Chitosan-Based Nanofibrous Scaffolds Macromol. *Macromol. Biosci.* **2008**, *8* (3), 239−246.
(56) Burwell, A. K.; Thula-Mata, T.; Gower, L. B.; Habeliz, S.; Kurylo, M.; Ho, S. P.; Chien, Y. C.; Cheng, J.; Cheng, N. F.; Gansky, S. A.; Marshall, S. J.; Marshall, G. W. Functional Remineralization of Dentin Lesions Using Polymer-Induced Liquid-Precursor Process. *PLoS One* **2012**, *7* (6), e38852.

DOI: 10.1021/acsami.5b07628
ACS Appl. Mater. Interfaces XXXX, XXX, XXX−XXX